Available online at www.sciencedirect.com
SCIENCE DIRECT®
Journal of Sound and Vibration 269 (2004) 327–343
JOURNAL OF SOUND AND VIBRATION
www.elsevier.com/locate/jsvi

On flow unsteadiness induced by structural vibration

Abdelkader Frendi*

Department of Mechanical and Aerospace Engineering, University of Alabama in Huntsville, N264 Technology Hall, Huntsville, AL 35899, USA

Received 28 June 2002; accepted 16 December 2002

Abstract

In this paper, the effects of structural vibration on flow unsteadiness are investigated numerically. A fully coupled model, that solves the unsteady flow equations as well as the dynamic equations of the structure, is used. Numerical experiments are carried-out for flow over a backward-facing step, where a large number of numerical and experimental data exist for comparisons. The flexible structure is upstream of the step and is excited by a plane acoustic wave from the side opposite to the flow. Three Reynolds number cases are studied: 300 for a laminar flow, 3000 for a transitional flow and 15 000 for a turbulent flow. The results obtained are in good agreement with experimental observations and show the strong coupling between structural vibration and the resulting flow unsteadiness.

1. Introduction

Fluid–structure interaction problems can be found in various engineering fields; civil, mechanical and aerospace to name a few. In aerospace as well as in many military applications, noise whatever its origin is undesirable. Since flow unsteadiness and structural vibration generate noise, it is therefore important to understand the noise generation mechanisms and devise control techniques to reduce or eliminate it. In this paper, a unique computation that couples a vibrating structure to the surrounding fluid flow is presented. The flow geometry considered is that of a backward-facing step and the flow conditions simulate the laminar, transitional and turbulent flow regimes.

Armaly et al. [1] carried-out an experimental and theoretical investigation of backward-facing step flow. They reported Laser–Doppler measurements of velocity distribution and reattachment

*Tel.: 256-824-6154; fax: 256-824-6758.
E-mail address: frendi@mae.uah.edu (A. Frendi).

0022-460X/03/$ - see front matter
doi:10.1016/S0022-460X(03)00075-0

length downstream of a single backward-facing step mounted in a two-dimensional channel for laminar, transitional and turbulent flows. The experimental results showed typical variations of the reattachment length with Reynolds number. In addition to the primary recirculation zone attached to the step, they observed additional regions on the top and bottom walls. Mullin et al. [2] studied experimentally airflow over a rearward-facing step with a free-stream velocity perturbed by a sinusoidal fluctuation of 1 Hz. They showed that the stability of the separated flow behind the step is strongly perturbed by the free-stream oscillations and that the position of reattachment of the turbulent boundary layer is dependent on the phase of the free-stream velocity. The time-dependent behavior of a reattaching shear layer behind a rearward-facing step was also experimentally studied by Driver et al. [3]. They showed that the majority of energy in the flow resides in frequencies characteristic of roll-up and pairing of vortical structures seen in free shear layers.

Recently, Huteau et al. [4] carried-out a detailed experimental study on the spatial–temporal movement of the reattachment and separation points in a two-dimensional backward-facing step flow with a bottom wall oscillating harmonically. They observed that the rate of variation of both points was strongly dependent on the wall oscillation. An experimental and numerical investigation of a 2-D backward-facing step flow was carried-out by Lee and Mateescu [5]. They measured, non-intrusively, the lengths of separation and reattachment on the upper and lower walls using closely spaced, multi-element hot-film sensor arrays. Their results compared well with previous experimental and computational results. Mateescu and Venditti [6] presented computational solutions for unsteady viscous flows in channels with a downstream-facing step, followed by an oscillating floor. The floor oscillations were specified as a product of sinusoidal oscillations in space and time.

In this paper, a fully coupled fluid–structure interaction model is used to compute a viscous flow past a backward-facing step followed by a flexible structure. A similar model was used by Frendi [7] to couple a supersonic turbulent boundary and a flexible structure. The numerical results obtained using this model were in very good agreement with those obtained experimentally by Maestrello [8]. In the past, the dominant approach to solving fluid–structure interaction problems was through the decoupling of the fluid and the structure [9–12]. The main assumption in this approach is that the structural vibrations do not alter the boundary layer flow, and therefore the fluid surface pressure is used as a forcing field on the structure without any feedback from the structure [13–15]. This assumption gives satisfactory results so long as the structural vibrations are small. However, when the surface pressure fluctuations are large, leading to a strong structural response, the feedback needs to be taken into account as shown by Frendi and Robinson [16].

In military as well as civilian applications, a low acoustic signature is a requirement for any new engineering machine. This, therefore, requires a better understanding of the mechanisms for noise generation and propagation. Flow induced structural vibration is one such noise generating mechanism and better models are required to understand it and find ways to control it.

The reminder of the paper is organized as follows: in the following section the mathematical model is derived, followed by a brief description of the methods of solution used. The results are discussed in Section 4 and some concluding remarks follow in Section 5.

2. Mathematical model

The fluid model used is based on the unsteady Reynolds averaged Navier–Stokes equations given by

$$\frac{\partial \rho}{\partial t} + \frac{\partial}{\partial x_i}(\rho U_i) = 0, \quad i = 1, 2, \tag{1}$$

$$\frac{\partial}{\partial t}(\rho U_i) + \frac{\partial}{\partial x_j}(\rho U_i U_j - \tau_{ij} + \rho \overline{u_i'' u_j''}) + \frac{\partial P}{\partial x_i} = 0, \quad i,j = 1, 2, \tag{2}$$

$$\frac{\partial E}{\partial t} + \frac{\partial}{\partial x_j}((E + P)U_j - \tau_{ij} U_j + \rho \overline{e'' u_j''} + \overline{p'' u_j''} - \overline{\tau_{ij} u_j''}) = 0, \tag{3}$$

$$P = (\gamma - 1)[E - \tfrac{1}{2}\rho(U_1^2 + U_2^2 + \overline{(u_1'')^2} + \overline{(u_1'')^2})]. \tag{4}$$

In Eqs. (1)–(4), (ρ, U_i, E, P) represent the unsteady means while the variables (u_i'', e'', p'') are the turbulent fluctuations. The total energy is defined as $E = P/(\gamma - 1) + \rho(U_1^2 + U_2^2)/2$. In Eqs. (2)

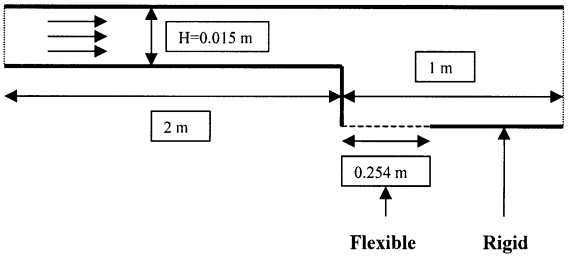

Fig. 1. Computational domain.

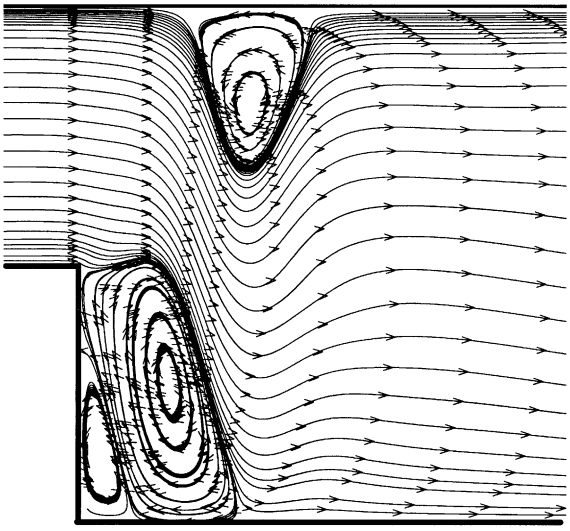

Fig. 2. Steady state streamtraces downstream of the backward-facing step for $Re = 300$ (▬▬, rigid wall).

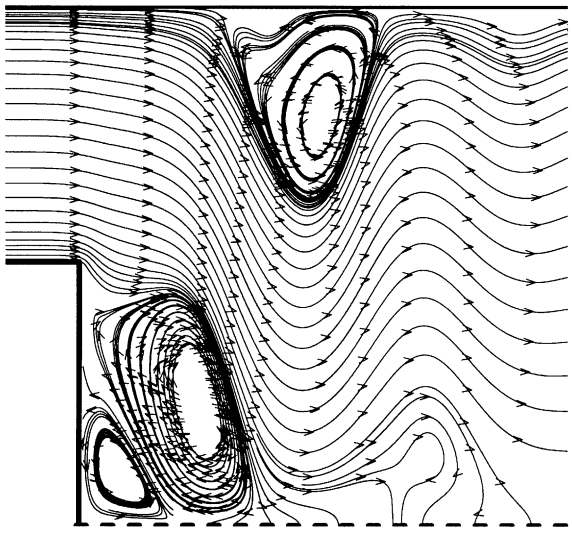

Fig. 3. Unsteady streamtraces downstream of the backward-facing step for $Re = 300$ (■■■■■■, flexible structure). Excitation frequency 138 Hz and amplitude $\varepsilon = 68.95\ \mathrm{N/m^2}$.

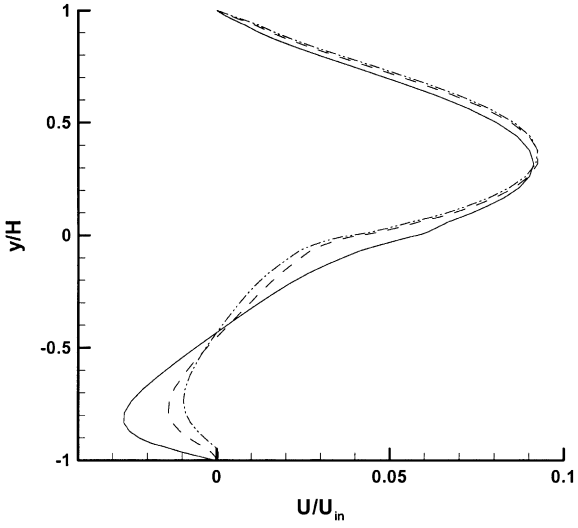

Fig. 4. Time variation of the non-dimensional mean velocity profile at the center of the flexible structure ($Re = 300$); ——, 0.00 s; - - - - - - -, 0.03 s; – - - – - - - - – –, 0.05 s. Excitation frequency 138 Hz and amplitude $\varepsilon = 68.95\ \mathrm{N/m^2}$.

and (3), τ_{ij} is the stress tensor given by

$$\tau_{ij} = \frac{M_\infty}{Re_L}\left[\mu\left(\frac{\partial U_i}{\partial x_j} + \frac{\partial U_j}{\partial x_i}\right) - \frac{2}{3}\mu\frac{\partial U_k}{\partial x_k}\delta_{ij}\right], \tag{5}$$

where M_∞, Re_L and μ are the free stream Mach number, Reynolds number and molecular viscosity, respectively. The term $\overline{\rho u_i'' u_j''}$ in Eq. (2) is the Reynolds stress and is modeled using the

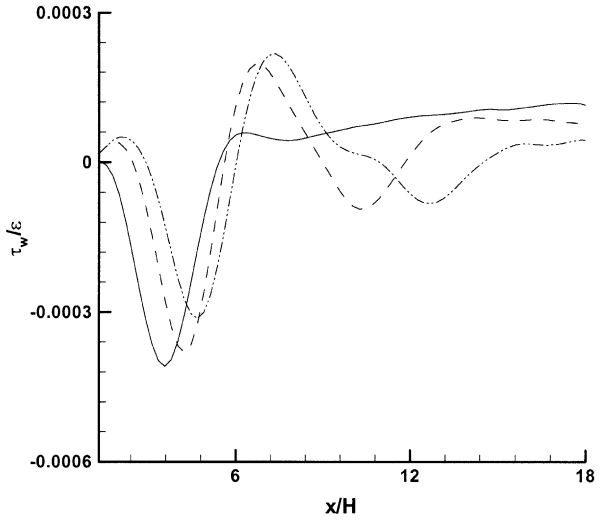

Fig. 5. Time variation of the non-dimensional fluid-wall-shear stress over the flexible structure ($Re = 300$): ——, 0.00 s; - - - - - - -, 0.03 s; – – – – – – – – –, 0.05 s. Excitation frequency 138 Hz and amplitude $\varepsilon = 68.95\ \mathrm{N/m^2}$.

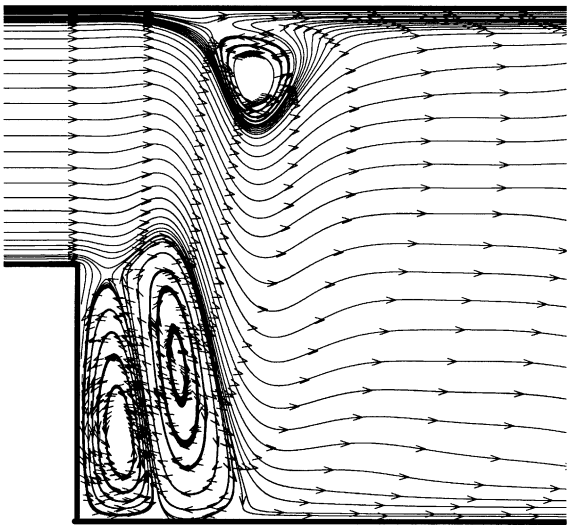

Fig. 6. Steady state streamtraces downstream of the backward-facing step for $Re = 3000$ (▬▬, rigid wall).

Boussinesq approximation as

$$\rho\overline{u_i'' u_j''} = \tfrac{2}{3}\rho k\delta_{ij} - 2\mu_t(S_{ij} - \tfrac{1}{3}S_{kk}\delta_{ij}), \tag{6}$$

where $k = \overline{u_i'' u_i''}/2$ is the turbulent kinetic energy, μ_t is the turbulent eddy viscosity, and S_{ij} is the mean strain-rate tensor given by

$$S_{ij} = \frac{1}{2}\left[\frac{\partial U_i}{\partial x_j} + \frac{\partial U_j}{\partial x_i}\right]. \tag{7}$$

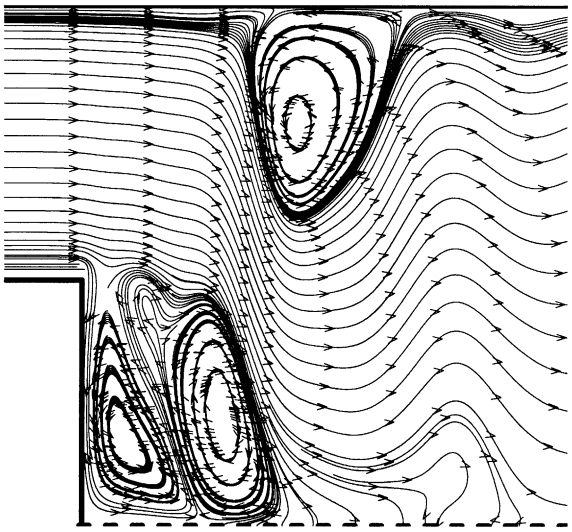

Fig. 7. Unsteady streamtraces downstream of the backward-facing step for $Re = 3000$ (▪▪▪▪▪▪, flexible structure). Excitation frequency 138 Hz and amplitude $\varepsilon = 68.95\ \mathrm{N/m^2}$.

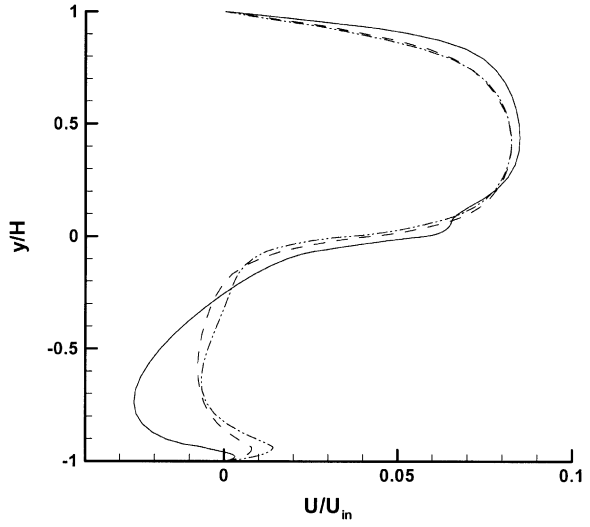

Fig. 8. Time variation of the non-dimensional mean velocity profile at the center of the flexible structure ($Re = 3000$): ——, 0.00 s; - - - - - - -, 0.03 s; – - - – - - – - - –, 0.05 s. Excitation frequency 138 Hz and amplitude $\varepsilon = 68.95\ \mathrm{N/m^2}$.

The turbulent eddy viscosity is obtained using the one equation closure model proposed by Spalart and Allmaras [17]. The terms $\overline{e''u_j''}, \overline{p''u_j''}$ and $\overline{\tau_{ij}u_j''}$ in the energy equation (3) need to be modelled.

In the fully coupled computations, a beam equation of the form

$$D\frac{\partial^4\eta}{\partial x^4} - \overline{N_x}\frac{\partial^2\eta}{\partial x^2} - \frac{\partial}{\partial x}\left[\tau_w\left(\eta + \frac{h}{2}\right)\right] + \rho_B h\frac{\partial^2\eta}{\partial t^2} + \Gamma\frac{\partial\eta}{\partial t} = \Delta p(t) \tag{8}$$

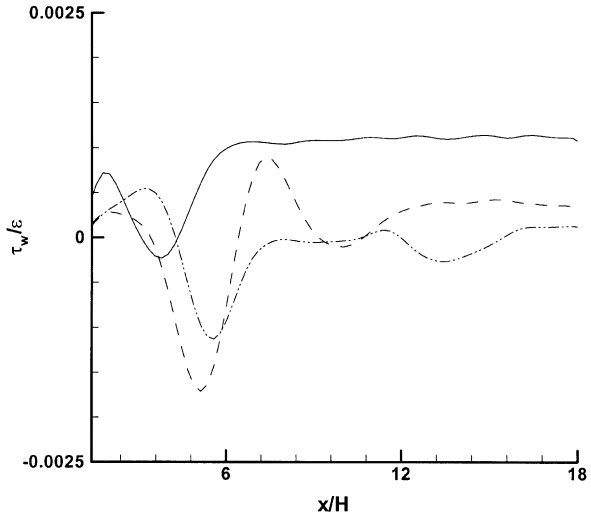

Fig. 9. Time variation of the non-dimensional fluid-wall-shear stress over the flexible structure ($Re = 3000$): ——, 0.00 s; - - - - - - - -, – – – – – – – – – –, 0.05 s. Excitation frequency 138 Hz and amplitude $\varepsilon = 68.95\ \mathrm{N/m^2}$.

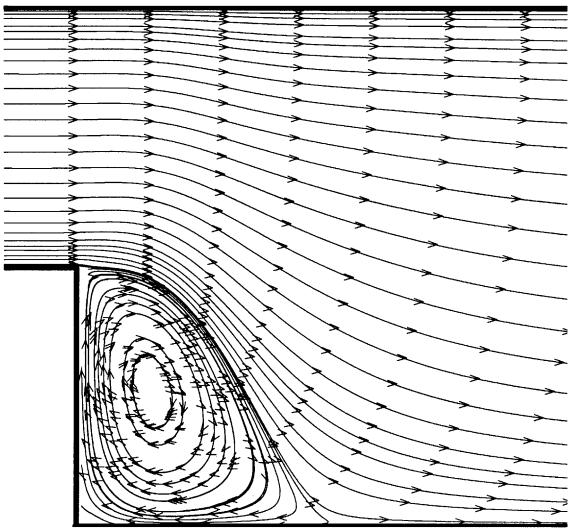

Fig. 10. Steady state streamtraces downstream of the backward-facing step for $Re = 15\,000$ (▬▬, rigid wall).

is used, where D is the beam stiffness, ρ_B its density, h the thickness, Γ the physical damping and η the out-of-plane displacement. In Eq. (8), $\overline{N_x}$ is the average tension in the beam due to bending and is defined as

$$\overline{N_x} = \frac{1}{2L} \int_{x_0}^{x_0+L} \left(\frac{\partial \eta}{\partial x} \right)^2 \mathrm{d}x \tag{9}$$

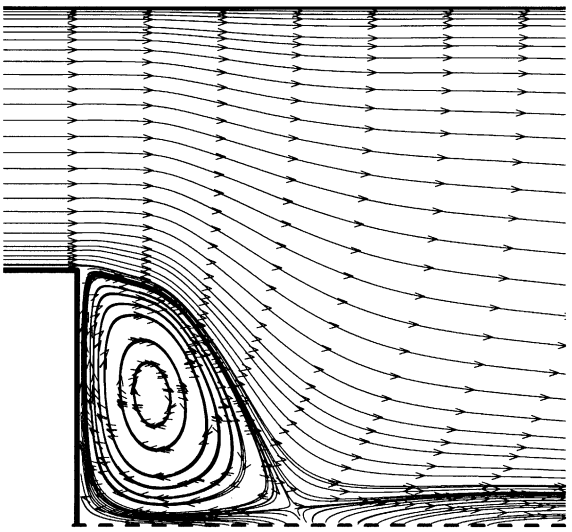

Fig. 11. Unsteady streamtraces downstream of the backward-facing step for $Re = 15\,000$ (■■■■■■, flexible structure). Excitation frequency 138 Hz and amplitudes $\varepsilon = 68.95\ \mathrm{N/m^2}$.

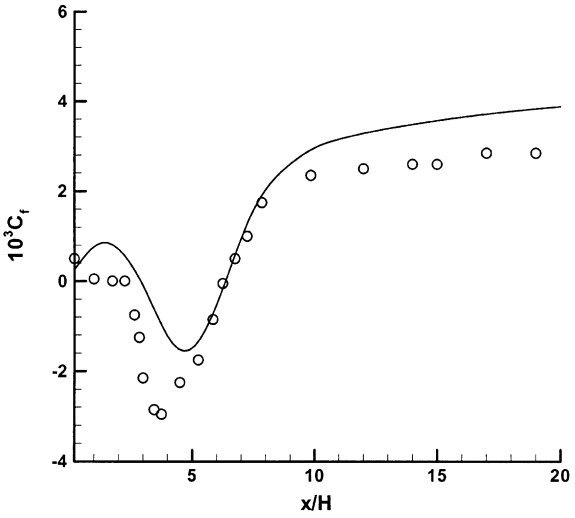

Fig. 12. Skin-friction coefficient downstream of the backward-facing step for $Re = 15\,000$: ○, experimental data (Adams et al.); ——, computed.

with L being the beam length and x_0 its origin. The forcing term, $\Delta p(t)$, in Eq. (8) is given by

$$\Delta p(t) = p^a - p^{b.l.} \tag{10}$$

with p^a being either plane acoustic waves exciting the beam from below at a given harmonic frequency, or a radiated acoustic pressure from the beam, and $p^{b.l.}$ the boundary layer pressure. In

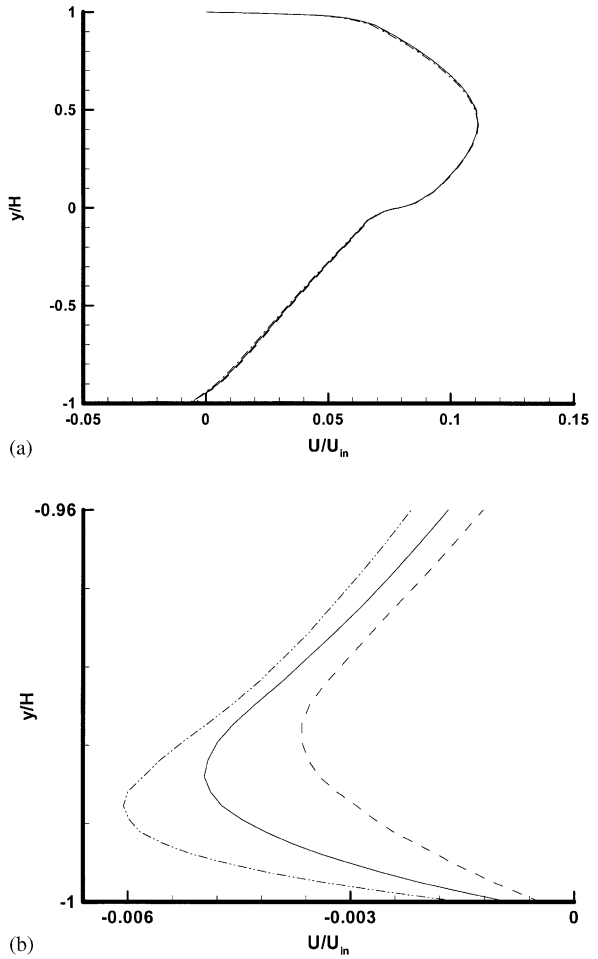

Fig. 13. Time variation of the non-dimensional mean velocity profile at the center of the flexible structure ($Re = 15\,000$); (a) entire channel (b) near the flexible structure. Excitation frequency 138 Hz and amplitude $\varepsilon = 68.95\ \mathrm{N/m^2}$. ——, 0.00 s; - - - - - - -, 0.03 s; – - - - - - - - - -, 0.05 s.

Eq. (8), τ_w is the fluid wall shear stress computed using

$$\tau_w = \mu_{eff} \left. \frac{\partial U}{\partial y} \right|_{y=0} \tag{11}$$

with μ_{eff} being the effective fluid viscosity.

3. Method of solution

Eqs. (1)–(7) are solved using the three-dimensional thin-layer Navier–Stokes code known as CFL3D [18]. The numerical method uses a second order accurate finite volume scheme. Low

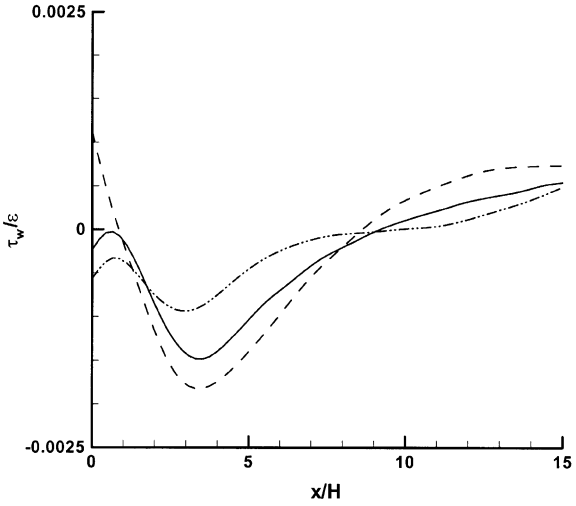

Fig. 14. Time variation of the non-dimensional fluid-wall-shear stress over the flexible structure ($Re = 15\,000$): ——, 0.00 s; - - - - - - -, 0.03 s; – - - – - - – - - –, 0.05 s. Excitation frequency 138 Hz and amplitude $\varepsilon = 68.95$ N/m^2.

Mach number preconditioning is used to insure convergence. At first a steady state solution is obtained, followed by the unsteady computation. When the code is used in the unsteady regime, a single time-stepping method (known as the "physical time sub-iteration or t-TS" due to Pulliam [19]) is used with 10 sub-iterations for each time step. The physical time step used in all the computations is 3×10^{-5} s. Reducing the time step did not result in any significant change of the solution. The choice of 10 sub-iterations gave the best convergence per time step. The beam equation (8) is integrated using an implicit finite difference scheme developed by Hoff and Pahl [20]. When the beam is excited from the side opposite to the flow, the forcing field is given by

$$p^a = \varepsilon \sin(\omega t), \tag{12}$$

where $\omega = 2\pi f$ is the forcing frequency, corresponding to one of the natural frequencies of the beam and ε the forcing amplitude. The wall boundary conditions are, $U = 0$ and $V = V_{Beam}$ over the flexible part of the wall and $V = 0$ over the rigid part.

Coupling between the beam and the fluid is obtained as follows. Using the previous time step's beam velocity as boundary conditions, the flow Eqs. (1)–(7) are integrated to obtain the new surface pressure field; these are then used to update the beam equation. This procedure is repeated at every time step.

4. Results and discussions

Results are obtained for a two-dimensional channel flow past a backward-facing step at three different Reynolds numbers (based on the step-height and the maximum inflow velocity); 300 for laminar flow, 3000 for transitional flow and 15 000 fully turbulent flow. Though Eqs. (1)–(7) are written for a compressible fluid, the computations are carried-out for an incompressible flow having a maximum Mach number of 0.03. The beam properties are: stiffness $D = 39$ N m, mass

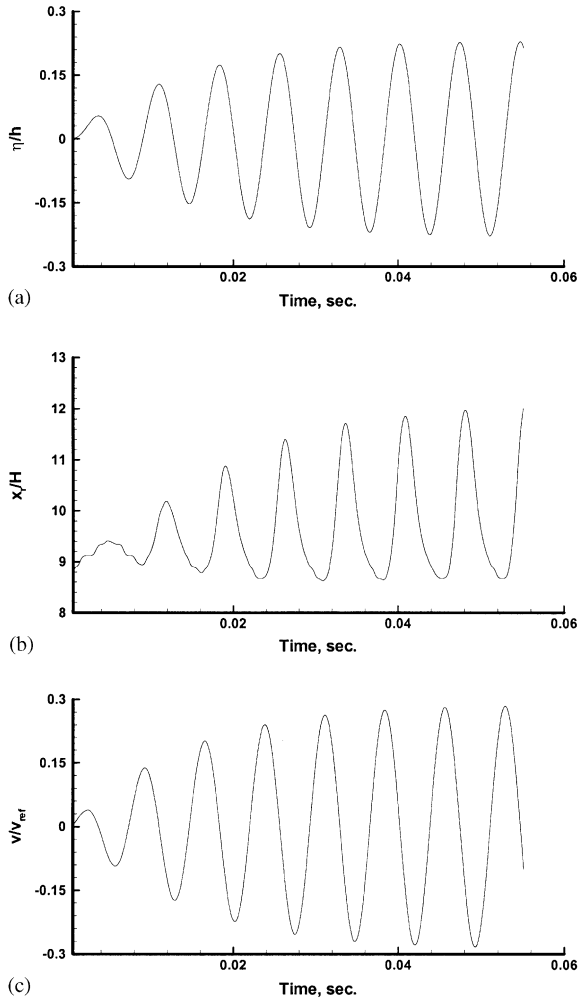

Fig. 15. Time histories of the non-dimensional (a) displacement, (b) flow reattachment point, and (c) structural velocity. Excitation frequency 138 Hz and amplitude $\varepsilon = 68.95\ \mathrm{N/m^2}$.

per unit area $\rho_B h = 6.28\ \mathrm{kg/m^2}$, structural damping $\Gamma = 14\ \mathrm{N\,s/m^3}$, thickness $h = 5.08 \times 10^{-4}$ m, and length $L = 0.254$ m. The first three natural frequencies are 138, 378 and 741 Hz. The computational domain shown in Fig. 1 is 2-m long upstream of the step and 1-m long downstream of it. The expansion ratio at the step is 2 with an upstream height of $H = 0.015$ m. After experimenting with several grid resolutions, the number of points used in all the computations are 501 in the streamwise direction, with 301 points located downstream of the step, and 161 and 81 in the vertical direction downstream and upstream of the step, respectively. Further grid refinement gave no significant change of the solution. In the unsteady computations, Eq. (12) is used to excite the structural vibrations with $\varepsilon = 68.95\ \mathrm{N/m^2}$ and using two different frequencies; 138 and 741 Hz corresponding to the first and third mode of the structure, respectively. In this section, nondimensional results will be presented, the wall shear stress is nondimensionalized with ε, the

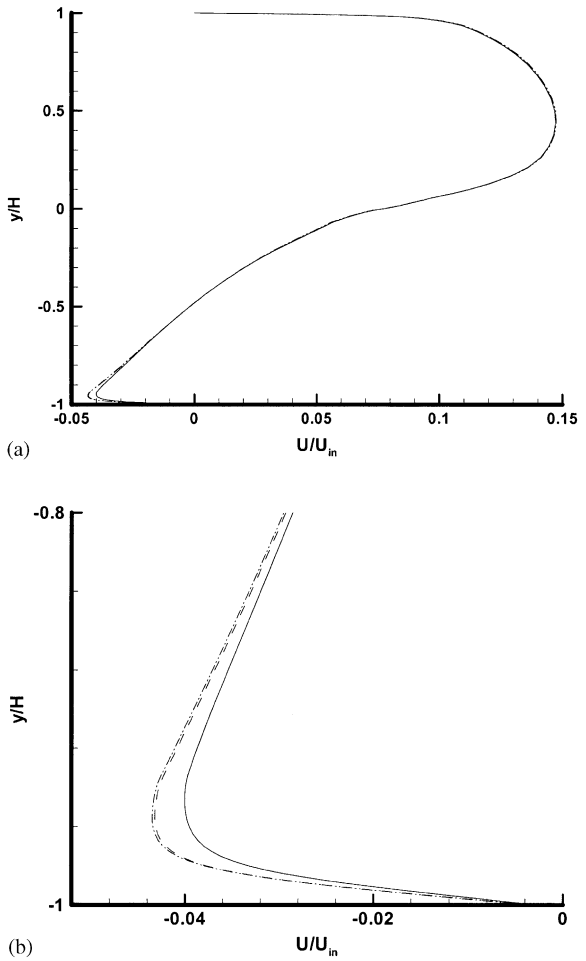

Fig. 16. Time variation of the non-dimensional mean velocity profile at the center of the flexible structure ($Re = 15\,000$); (a) entire channel (b) near the flexible structure. Excitation frequency 740 Hz and amplitude $\varepsilon = 68.95\ \mathrm{N/m^2}$. ——, 0.00 s; - - - - - - -, 0.03 s; — - - — - - — - - —, 0.05 s.

mean flow velocity by $U_{in} = 72$ m/s, the structural vibration velocity at the center of the beam by $V_{ref} = 2.54 \times 10^{-5}$ m/s, the out-of-plane structural displacement by the beam thickness h, and the x and y co-ordinates by the step height H.

Fig. 2 shows the steady state streamtraces for the laminar case, $Re = 300$. In this case the flow field is characterized by the presence of a large and small recirculation bubble ahead of the step on the lower wall and another recirculation bubble on the upper wall. The location of the upper wall recirculation bubble is slightly downstream of the bottom wall bubbles. This result is in agreement with what was observed experimentally and obtained numerically [1,6]. In the unsteady computation (Fig. 3) the flow-field downstream of the step is changed. The figure shows the changes to be characterized by the stretching of the top and bottom bubbles due to the downward motion of the structure. In addition, a new recirculation bubble is shown on the bottom wall over

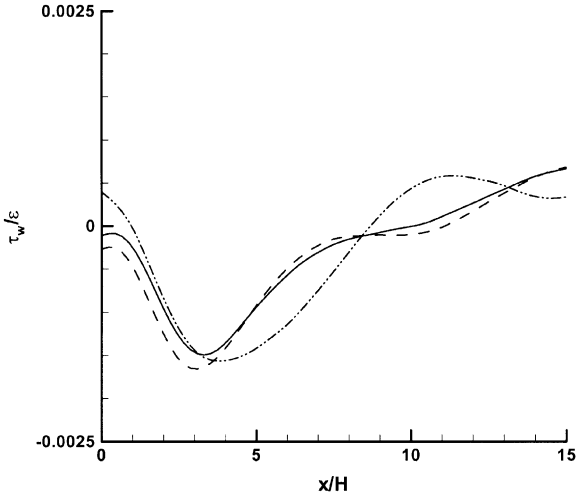

Fig. 17. Time variation of the non-dimensional fluid-wall-shear stress over the flexible structure ($Re = 15\,000$): ——, 0.00 s; - - - - - - -, 0.03 s; — - - — - - — - - —, 0.05 s. Excitation frequency 740 Hz and amplitude $\varepsilon = 68.95$ N/m^2.

the flexible structure and downstream of the previously obtained bubbles. Fig. 4 shows the time variation of the non-dimensional mean velocity profile at the center of the flexible structure. The figure shows that as time increases, the magnitude of the negative velocity near the flexible structure is reduced, and for $t = 0.05$ s the velocity becomes slightly positive. The variation with time of the non-dimensional wall shear stress over the flexible structure is shown in Fig. 5. The solid line corresponding to the steady state value shows the presence of one dominant bubble. Whereas at other times, the wall shear stress exhibits a more complex shape indicating the presence of more recirculation bubbles. These results are in agreement with those of Lee and Mateescu [5].

In the transitional Reynolds number case, $Re = 3000$, Fig. 6 shows the presence of three recirculation bubbles. In this case, the bottom two bubbles are larger, while the top bubble is smaller than the laminar one. Fig. 7 shows the unsteady result corresponding to the transitional Reynolds number case. Similar to the laminar case, the three bubbles are stretched and a new bubble has formed over the flexible structure downstream of the steady state bubbles of Fig. 6. In addition, a new small recirculation bubble seems to be forming on top of the two bottom wall bubbles adjacent to the step. The time variation of the non-dimensional mean velocity profile at the center of the flexible structure is shown in Fig. 8. Similar to the laminar case, significant changes are taking place near the flexible structure. The non-dimensional wall shear stress (Fig. 9) shows the presence of two bubbles at steady state (solid line). The figure shows that downstream of the second bubble the wall shear stress is nearly constant. However, this is not the case when structural vibration is introduced as indicated by the other two curves.

In the turbulent flow regime, $Re = 15\,000$, only one dominant bubble is obtained downstream of the step on the bottom wall (Fig. 10). The bubble is larger in size than the two laminar or transitional bubbles combined. In the unsteady case, (Fig. 11) the bubble shrunk slightly due to the upward motion of the flexible structure. In addition, the fluid is being pushed upward by the

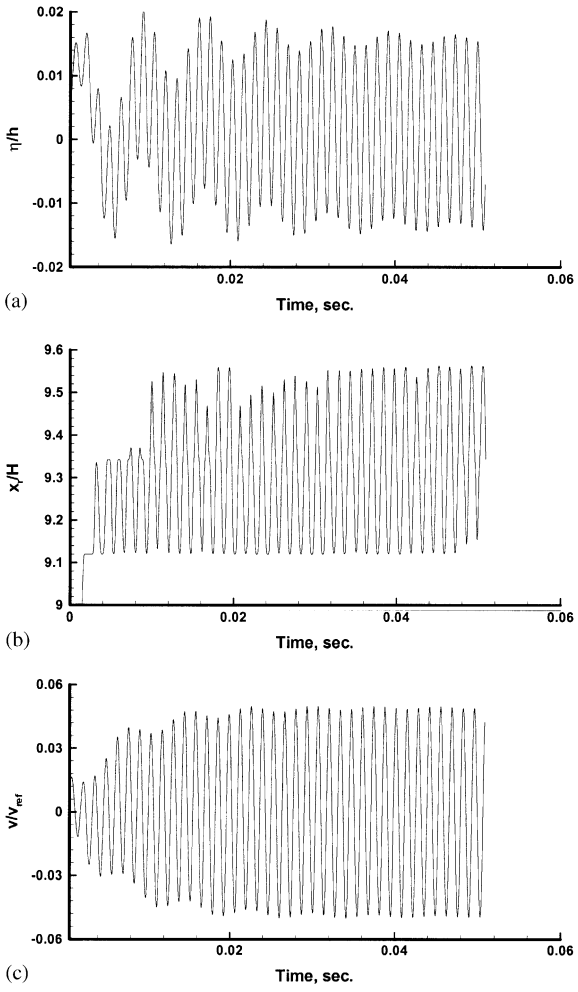

Fig. 18. Time histories of the non-dimensional (a) displacement, (b) flow reattachment point, and (c) structural velocity. Excitation frequency 740 Hz and amplitude $\varepsilon = 68.95\ \mathrm{N/m^2}$.

flexible structure as indicated by the streamtraces originating from the surface. Fig. 12 shows a comparison between the computed friction coefficient and that measured by Adams et al. [21] downstream of the backward-facing step at nearly similar conditions. There is a good overall agreement between the two results. In addition, the locations of the reattachment points predicted in the current computations are in good agreement with those reported in the literature. Specifically, the present computations find this point to be at $5.5H$, $6H$ and $7.5H$ from the step for the laminar, transitional and turbulent cases, respectively. In the literature, various authors give reattachment locations between $4H$ and $8H$ for the different flow conditions (see Ref. [6] for example). The non-dimensional mean velocity profile at the center of the flexible structure at three different times is shown in Fig. 13. Fig. 13(a) shows the velocity profile for the entire channel.

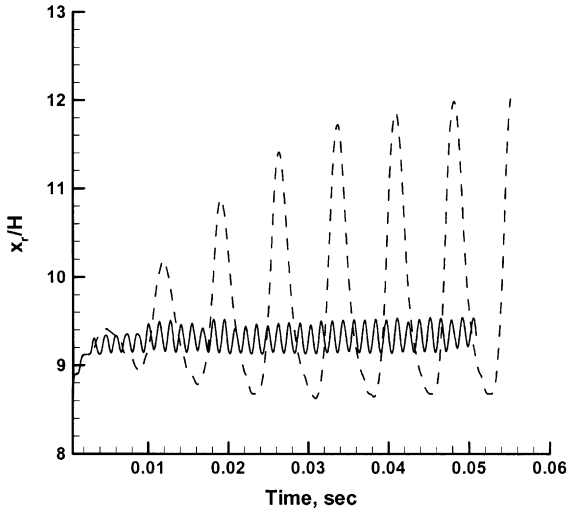

Fig. 19. Comparison of the time histories of the reattachment point obtained using excitations frequencies of: - - - - - - -, 138 Hz (1st mode) and ——, 740 Hz (3rd mode) and an excitation amplitude of $\varepsilon = 68.95\ \mathrm{N/m^2}$.

Small changes can be seen due to the presence of the flexible structure. However, the near-wall behavior is better shown by Fig. 13(b), where significant changes in the velocity profile are shown. Fig. 14 shows the variation of the non-dimensional wall shear stress over the flexible structure at three different times. The figure shows the existence of a small bubble at the bottom of the step in addition to the big bubble. This bubble is strongly affected by the surface vibration since it is present at times 0 and 0.05 s and absent at time 0.03 s. As to the big recirculation bubble, it shrinks and expands as the surface vibrates.

Figs. 15(a)–(c) show the time histories of the non-dimensional out-of-plane displacement at the center of the flexible structure (Fig. 15(a)) and its non-dimensional velocity (Fig. 15(c)). In addition, the oscillation of the non-dimensional downstream location of the reattachment point is shown in Fig. 15(b). The figure shows that as the structure oscillates the reattachment point is either closer to or further away from the step. The closest reattachment point to the step occurs with the maximum structural velocity. One of the parameters that can significantly affect the flow is the frequency of the structural vibration. Increasing the excitation frequency to 741 Hz, corresponding to the third mode of the beam, resulted in a reduction in the fluctuation of the non-dimensional mean velocity profile as shown by Figs. 16(a) and (b). Compared to Fig. 16(a), Fig. 16(b) shows less variation with time. Similarly, the non-dimensional wall shear stress, Fig. 17, shows less variation than that shown in Fig. 14. This result is confirmed by Fig. 18; which shows the time history of the non-dimensional displacement (Fig. 18(a)) non-dimensional downstream location of the reattachment point (Fig. 18(b)) and the non-dimensional velocity at the center of the structure (Fig. 18(c)). The figure shows a higher frequency of oscillation, but a lower oscillation amplitude. A comparison of time histories of the non-dimensional downstream location of the reattachment point obtained using the two different frequencies is shown in Fig. 19. The figure shows that the location of the reattachment point exhibits a large variation when the first vibration mode is used.

5. Concluding remarks

Results have been presented on the effects of structural vibration on the surrounding flow field. In all the flow regimes studied, laminar, transitional and turbulent, the structural vibration is found to introduce significant changes in the flow field. The size and shape of the various recirculation bubbles is found to be strongly affected and oscillate at the same frequency as that of the structure. In addition, the reattachment point oscillates at the same frequency as that of the structural vibrations. These results are in good agreement with previous experimental and numerical studies.

Acknowledgements

Support for this work has been provided by ONR Grant N00014-01-1-0128 with Dr. Luise Couchman as the technical monitor.

References

[1] B.F. Armaly, F. Durst, J.C.F. Pereira, B. Schonung, Experimental and theoretical investigation of backward-facing step flow, Journal of Fluid Mechanics 127 (1983) 473–495.
[2] T. Mullin, C.A. Greated, I. Grant, Pulsating flow over a step, Physics of Fluids 23 (4) (1980) 669–674.
[3] D.M. Driver, H. Lee Seegmiller, J.G. Marvin, Time-dependent behavior of a reattaching shear layer, American Institute of Aeronautics and Astronautics Journal 25 (7) (1987) 914–919.
[4] F. Huteau, T. Lee, D. Mateescu, Flow past a 2-D backward-facing step with an oscillating wall, Journal of Fluids and Structures 14 (2000) 691–696.
[5] T. Lee, D. Mateescu, Experimental and numerical investigation of a 2-D backward-facing step flow, Journal of Fluids and Structures 12 (1998) 703–716.
[6] D. Mateescu, D.A. Venditi, Unsteady confined viscous flows with oscillating walls and multiple separation regions over a downstream-facing step, Journal of Fluids and Structures 15 (2001) 1187–1205.
[7] A. Frendi, Coupling between a supersonic turbulent boundary layer and a flexible structure, American Institute of Aeronautics and Astronautics Journal 35 (1) (1997) 58–66.
[8] L. Maestrello, Radiation from and panel response to a supersonic turbulent boundary layer, Journal of Sound and Vibration 10 (2) (1969) 261–295.
[9] G.M. Corcos, Resolution of pressure in turbulence, Journal of Acoustical Society of America 35 (2) (1963) 192–198.
[10] J.E. Ffowcs Williams, Boundary layer pressures and the corcos model: a development to incorporate low wavenumber constraints, Journal of Fluid Mechanics 125 (1982) 9–25.
[11] D.M. Chase, Modeling the wavenumber–frequency spectrum of turbulent boundary layer wall pressure, Journal of Sound and Vibration 70 (1) (1980) 29–67.
[12] A.L. Laganelli, A. Martellucci, L.L. Shaw, Wall pressure fluctuations in attached boundary layer flows, American Institute of Aeronautics and Astronautics Journal 21 (4) (1983) 495–502.
[13] B.M. Efimtsov, Characteristics of the field of turbulent wall pressure fluctuations at large Reynolds numbers, Soviet Physical Acoustics 28 (4) (1982) 289–292.
[14] W.K. Blake, Turbulent boundary layer wall pressure fluctuations on smooth and rough walls, Journal of Fluid Mechanics 44 (4) (1970) 637–660.
[15] W.R. Graham, A comparison of models for the wavenumber–frequency spectrum of turbulent boundary layer pressure, Proceedings of the First AIAA/CEAS Conference on Aeroacoustics (Munich, Germany), 1994, pp. 711–720.

[16] A. Frendi, J. Robinson, Effect of acoustic coupling on random and harmonic plate vibrations, American Institute of Aeronautics and Astronautics Journal 31 (11) (1993) 1992–1997.
[17] P. Spalart, S. Allmaras, A one-equation turbulence model for aerodynamic flows, La Recherche Aerospatiale 1 (1994) 5–21.
[18] C. Rumsey, J. Thomas, G. Warren, G. Liu, Upwind Navier–Stokes solutions for separated periodic flows, AIAA 86-0247, 1986.
[19] T. Pulliam, Time accuracy and the use of implicit methods, AIAA 93-3360, 1993.
[20] C. Hoff, P.J. Pahl, Development of an implicit method with numerical dissipation from a generalized single-step algorithm for structural dynamics, Computer Methods in Applied Mechanics and Engineering 67 (2) (1988) 367–385.
[21] E.W. Adams, J.P. Johnston, J.K. Eaton, Report MD-43, Department of Mechanical Engineering, Stanford University, 1984.